Denoising Of Poisson-Corrupted Biopsy Images

Ahmed Loay ElSayed
Biomedical Engineering Department
Cairo University
ahmed.ali041@eng-st.cu.edu.eg

Sarah Sameh Mohamed
Biomedical Engineering Department
Cairo University
sarah.mohamed03@eng-st.cu.edu.eg

Alhussien Ayman Hanafy
Biomedical Engineering Department
Cairo University
alhussien.mohamed04@eng-st.cu.edu.eg

Lyan Ahmed Mohsen
Biomedical Engineering Department
Cairo University
lyan.ahmed03@eng-st.cu.edu.eg

Mariam Sherif Mohamed
Biomedical Engineering Department
Cairo University
mariam.awwad04@eng-st.cu.edu.eg

***Abstract*— Microscopic biopsies are essential in the early identification of lung cancer. However, the diagnostic utility of these images is often compromised by Poisson noise, which degrades image quality and hinders accurate interpretation by medical specialists. This study aims to address this challenge by reducing Poisson noise while preserving critical features such as edges and boundaries and enhancing abnormal regions. To achieve this, a novel approach combining fourth-order partial differential equations with Ant Colony Optimization is proposed.**

I. Introduction

Lung cancer remains one of the leading causes of mortality worldwide. While it can sometimes be inherited, it is more commonly caused by specific disorders or prolonged exposure to toxins such as cigarette smoke [1]. Early diagnosis is critical to reducing the mortality rate associated with this fatal disease. Diagnostic efforts often rely on imaging modalities such as X-rays, computed tomography (CT), magnetic resonance imaging (MRI), and tissue sampling through biopsy procedures [2]. Microscopic biopsy, in particular, is a widely used method that provides precise early identification of lung cancer through digital images. However, a significant challenge arises in the form of photon noise. This noise, which follows a Poisson distribution, is multiplicative in nature and caused by random fluctuations of photons hitting the sensor during image acquisition [3]. The presence of such noise not only degrades image quality but also hinders the extraction of meaningful information, thereby complicating the early diagnosis of lung cancer. To address this issue, a novel approach combining fourth-order partial differential equations (PDEs) with Ant Colony Optimization (ACO) [4] has been proposed. This method aims to effectively denoise the images while preserving critical structural features, enhancing the diagnostic utility of microscopic biopsy images.

II. Problem Definition

First, Biopsy images of lung and colon cancer are often corrupted by **Poisson noise** [5]—a multiplicative noise arising from photon fluctuations during image acquisition. This degradation reduces the interpretability of images for doctors and impairs downstream image processing tasks, such as segmentation and classification.

Existing methods for denoising, including spatial filters, statistical techniques, and PDE-based approaches, often fail to preserve fine details, restore edges, or address parameter tuning complexities. These issues result in over-smoothed images or loss of critical high-frequency information.

The general problem can be shown in the following equation:

$$u_o = u*\beta 2 + \beta 1 \quad (1)$$

- → u_o: The observed noisy image.
- → u: The original microscopic biopsy image.
- → β2: Poisson-distributed multiplicative noise.
- → β1: Additive noise from machine calibration, assumed negligible in this work.

Since additive noise is neglected, the equation can be written as follows and said to be the overall equation of image generation:

$$u_o = u*\beta 2 = \text{Poisson}*u \quad (2)$$

In order to restore u from u_o, the negative log-likelihood (NLL) [5] of the Poisson distribution is minimized:

$$\operatorname{argmin}_{u\geq 0}\left(-\ln\left(\prod_{u=1}^{n}\frac{u^{u_0}e^{-u}}{u_0!}\right)\right) \quad (3)$$

Where, the function *argmin* $u\geq 0$ signifies the minimization of the likelihood function. Simplified it will be written as:

$$\operatorname{argmin}_{u\geq 0}\left(-l(u;u_1,u_2,u_3,\dots,u_n)\right) = \sum_{u=1}^{n}(u-u_0\ln u) \quad (4)$$

However, this formulation alone restores attribute information but fails in removing Poisson noise properly. Hence, it is integrated into a fourth-order partial differential equation (FPDE)-based regularization framework [6]:

$$E(u) = \operatorname{argmin}_{u\geq 0}\left\{\int_{\Omega}[u_{\text{MLE}} + \nabla^2\cdot(c(||\nabla^2 u||)\nabla^2 u)]d\Omega\right\} \quad (5)$$

- → Ω: Image domain.
- → uMLE: Maximum likelihood estimation-based restoration [7].
- → c: Diffusion coefficient which can be defined as:

$$c(||\nabla^2 u||) = \frac{1}{1+\left(||\frac{\nabla^2 u}{k}||\right)^2} \quad (6)$$

- → ∇: Laplacian operator for edge restoration also known as the gradient of the image.
- → k: Edge threshold constraint, automatically computed using the mean absolute deviation (MAD) of the image:

$$k_{\text{MAD}} = \text{median}(|u(i,j)-\mu|) \quad (7)$$

- → μ: Mean of the image.

And since this combination leads to an ill-posed problem, a regularization parameter λ [8] is proposed for balancing noise removal, detail preservation and smoothness control which is given by:

$$\lambda = \frac{\sqrt{\sigma^2}}{\mu} \quad (8)$$

→ σ: The standard deviation of the image.

Objectives:

1. Denoising: Eliminate Poisson noise from microscopic biopsy images.
2. Restoration: Preserve edges and fine details using the integrated maximum likelihood estimation.
3. Automation: Replace manual parameter tuning with automated methods (e.g., MAD for diffusion coefficient).
4. Optimization: Tune control parameters via ant colony optimization (ACO), using peak signal-to-noise ratio (PSNR) as the fitness function.

III. Methodology

To solve the problem of microscopic biopsy images containing photon noise (Poisson noise), a novel Ant Colony Optimization-Based Reformed Fourth-Order Partial Differential Equation (ACO-RFPDE) is proposed [9].

An effective framework combining Fourth-Order Partial Differential Equation (FPDE), Maximum Likelihood Estimation (MLE), and Ant Colony Optimization (ACO) is introduced to eliminate noise and enhance the quality of microscopic biopsy images, with the potential integration of an assistive AI model.

A. Framework Design and Development

To design and develop the RFPDE, the Classical Fourth-Order PDE (CFPDE) is integrated with MLE to restore the image. The diffusion coefficient in the CFPDE is automated with the help of the Median Absolute Deviation (MAD) of images. Finally, ACO is applied to tune the controlling parameters of the RFPDE.

→ Modeling Noise: By identifying a relationship between the noisy image (u_o), the original microscopic image (u), and Poisson noise, neglecting any additive noise, the noise model is formulated.

→ MLE Application: The MLE [7] estimates parameters by either maximizing the likelihood function or minimizing the negative log-likelihood function. MLE provides a restored image based on the distribution function but has limited ability to properly remove Poisson noise.

→ Integration of CFPDE with MLE: The CFPDE, which is an iterative method based on PDE principles, is combined with MLE. A regularization parameter (λ) [8] is introduced to balance noise removal and control the smoothness of the image.

→ Numerical Approach: The output equation is discretized using the finite difference scheme, a numerical approach that ensures computational stability.

→ Incorporating ACO: ACO is a nature-inspired optimization algorithm mimicking the foraging behavior of ants. It helps optimize the controlling parameters of the RFPDE, including the time constant (Δt), number of iterations (n), and regularization parameter (λ). ACO simulates how ants find the shortest path between their colony and a food source using pheromone trails, optimizing the process dynamically.

B. Iterative Process for Image Denoising

During the iterative process:

→ Pixel Updates: Pixel values are updated using finite difference approximations for spatial gradients and Laplacians.

→ Guiding Parameters: The time constant (Δt), regularization parameter (λ), and diffusion coefficient ($c(\|\nabla^2 u\|)$) guide the iterative process.

The iterative process generates a partially restored image. ACO is then applied to refine the time constant (Δt) and number of iterations (n) for the RFPDE to further enhance image quality.

C. Final Steps

→ Stopping Criterion: The ACO process iterates until a stopping criterion is met (e.g., maximum iterations or optimal parameter values).

→ Optimized Output: The optimized parameters from ACO are combined with the RFPDE to produce the final restored and enhanced image.

→ Assistive AI Model: The enhanced image could be provided to an assistive AI model for further enhancement, achieving the best possible output for microscopic biopsy analysis.

IV. Solution And Models

In this section, the proposed solution is thoroughly analyzed and discussed in detail.

A. Follow up: PDE Equations

The mean of the image which was involved in multiple calculations until now can be calculated as [10]:

$$\mu = \frac{1}{P \cdot Q} \sum_{i=1}^{P} \sum_{j=1}^{Q} u(i,j) \quad (9)$$

where (*P*Q*) are the image size.

To obtain the minimized value of NLL, the Eq. (4) is differentiated with respect to *u* and equated to zero. Thus, the NLL-based MLE is:

$$u_{\text{MLE}} = \frac{u_o - u}{u_o} \quad (10)$$

Where u_{MLE} is the maximum likelihood estimation and u_o, u are the noisy image and the original microscopic image respectively.

In order to obtain the proposed RFPDE, Eq. (5) is minimized by Euler-Lagrange and gradient decent [11]. The minimized form offers denoising as well as restoration of microscopic biopsy image. It turned as:

$$\frac{\partial u}{\partial t} = \frac{1}{\lambda} \cdot \frac{(u_o - u)}{u} + \nabla^2 \cdot (c_{\text{MAD}}(||\nabla^2 u||)\nabla^2 u) \quad (11)$$

Finite difference scheme is applied the equation (11) and it may be expressed as the following after rearrangement:

$$u_{ij}^{n+1} = u_{ij}^{n} + \Delta t\left[\frac{1}{\lambda}\left(\frac{u_o - u_{ij}^{n}}{u_{ij}^{n}}\right) + \nabla^2\left(c_{\text{MAD}}\left(||\nabla^2 u_{ij}^{n}||\right)\nabla^2 u_{ij}^{n}\right)\right] (12)$$

- → Δt: The time constant.
- → n: The number of iterations.
- → λ: The regularization parameter.
- → $u_{ij}^{n+1} = u_{RFPDE}$, which shows the reformed fourth order partial differential equation.

B. ACO Equations

Ant Colony Optimization (ACO) is employed to optimize the Regularized Fourth-Order Partial Differential Equation (RFPDE) for image denoising. The ACO framework uses pheromone trails and heuristic information to guide artificial ants toward optimal solutions. The following section outlines the key mathematical formulations, including transition probabilities, pheromone updates, and the PSNR-based fitness function used to evaluate the denoising performance.

The probability of selecting the m^{th} node as the endpoint by the r^{th} ant placed at the n^{th} node is formulated [12] as follows:

$$\text{P(t)}_{\text{mn}}^{\text{r}} = \begin{cases} \frac{[\tau(t)_{mn}]^{\alpha}[\eta_{mn}]^{\beta}}{\sum[\tau(t)_{mn}]^{\alpha}[\eta_{mn}]^{\beta}}; \ if\ m\ is\ connected\ to\ n \\ 0; \ otherwise \end{cases} (13)$$

- → $\tau(t)_{mn}$: The amount of pheromone trail between node m and n.
- → η_{mn}: Is heuristic information.
- → (α, β) are constants.

The amount of pheromone left behind by each ant is calculated as:

$$\Delta\tau(\text{t}, \text{t}+1)_{mn}^{r} = \begin{cases} \frac{\text{fitness}(\text{Z}^{\text{r}})}{\text{X}}; \ if\ (m,n) \in path\ of\ r^{th}\ ant \\ 0; \ otherwise \end{cases} (14)$$

- → $\Delta\tau(\text{t}, \text{t}+1)_{mn}^{r}$: It is the amount of pheromone deposited on the edge between nodes m and n by the r^{th} ant during the time interval [t, t+1]. Its value is updated only for the edges that the ant traversed during its path; otherwise, it is zero.
- → Z^{r}: Represents the complete path taken by the r^{th} ant during a single iteration.
- → $\text{Fitness}(\text{Z}^{\text{r}})$: A function that evaluates the quality or effectiveness of the path Z^{r}. Higher fitness values indicate better solutions, leading to more pheromone being deposited.
- → X: A fixed value that normalizes the amount of pheromone deposited.

At the end of an iteration, the cumulative pheromone left by all ants is given by:

$$\Delta\tau(\text{t}, \text{t}+1)_{mn} = \sum_{r=1}^{l} \Delta\tau(\text{t}, \text{t}+1)_{mn}^{r} (15)$$

Where l is the total number of ants used in the optimization process.
The following equation is used to revise the pheromone quantity for the subsequent iteration:

$$\tau(\text{t}, \text{t}+1)_{mn} = (1-\rho)\cdot\tau(\text{t})_{mn} + \Delta\tau(\text{t}, \text{t}+1)_{mn} (16)$$

- → $\tau(\text{t})_{mn}$: The pheromone value for the edge (m, n) at the start of the current iteration t.
- → ρ: The evaporation factor ∈ [0, 1]. It represents the rate at which pheromone decays over time.
- → $(1-\rho)$: The fraction of pheromone that remains on the edge after evaporation.

In order to tune the RFPDE by ACO, PSNR has been utilized as fitness function. It was used as a fitness function since higher values of PSNR mean a better denoised image. The mathematical equation is as follows:

$$\hat{z}_{fitness} = \text{argmax}\left(f(Z^{r})_{\text{PSNR}}\right) (17)$$

Where $\hat{z}_{fitness}$ shows the fitness in terms of PSNR values.

The following two equations (18) and (19) refer to how PSNR is calculated:

$$f(Z^{r})_{\text{MSE}} = \frac{1}{P\cdot Q}\sum_{i=0}^{P-1}\sum_{j=0}^{Q-1}\left(u_{\text{RFPDE}}(i,j) - u_{\text{ref}}(i,j)\right)^2 (18)$$

- → P and Q are the height and width respectively.
- → $u_{\text{RFPDE}}(i,j)$: The pixel intensity of the denoised image at location (i, j).
- → $u_{\text{ref}}(i,j)$: The pixel intensity of the reference (noise-free) image at location (i, j).

$$\hat{z}_{fitness} = \text{argmax}\left(f(Z^{r})_{\text{PSNR}}\right) = 10\log_{10}\left(\frac{(L-1)^2}{\text{MSE}(u_{\text{RFPDE}}, u_{\text{ref}})}\right) (19)$$

- → L is the maximum gray-level intensity
- → MSE: The Mean Squared Error value, calculated in equation (18). Represents the average squared difference between the denoised image and the reference image.

→ *Assistive AI Model*

As a final step, an assistive AI model, BM3D (Block Matching and 3D Filtering), was utilized for further enhancement of the restored image processed by the ACO-RFPDE framework. BM3D, implemented as part of a Python library [13], is a state-of-the-art algorithm designed for image denoising and enhancement. While ACO-RFPDE effectively reduces Poisson noise and preserves critical features, residual noise may still persist. The application of BM3D addresses this by enhancing the image further, ensuring improved quality and clarity for subsequent analysis.

V. RESULTS

The ACO-RFPDE framework coupled with BM3D was applied to images with noise levels ranging from 1 (very low) to 8 (extremely high). The difference between these noise levels depends on the scaling factor, which determines the intensity of the noise. At higher scaling factors (low noise levels), the noisy image closely resembles the original, with only small random variations in pixel intensities. In contrast, lower scaling factors (high noise levels) simulate darker images with fewer photons, where Poisson noise becomes more prominent as the peak signal-to-noise ratio (PSNR) decreases. As noise increases, it becomes more visible, especially in darker regions, and eventually obscures fine details, causing significant deviations in pixel values.

The model's performance was evaluated based on its ability to reduce noise effectively. Metrics such as Peak Signal-to-Noise Ratio (PSNR) and Structural Similarity Index (SSIM) were used for quantitative assessment, while qualitative visual comparisons ensured that important image features were preserved, and overall quality was improved. Two noise levels, 4 and 6, were selected to analyze the outcomes. At noise level 4, the image appeared noisy but retained sufficient brightness and detail with a noise percentage of approximately 25%. In contrast, at noise level 6, the image became significantly darker, and many features were obscured due to the higher intensity of Poisson noise corresponding to a noise percentage of approximately 75%. Tests were conducted on multiple cancer biopsy images obtained from the LC25000 dataset [14], including both lung and colon biopsies. Each image was evaluated at multiple noise levels; however, only two levels will be discussed in the following section. Qualitative analysis is straightforward in this context, as the noise is highly evident in the images, and the denoising results are visually distinct.

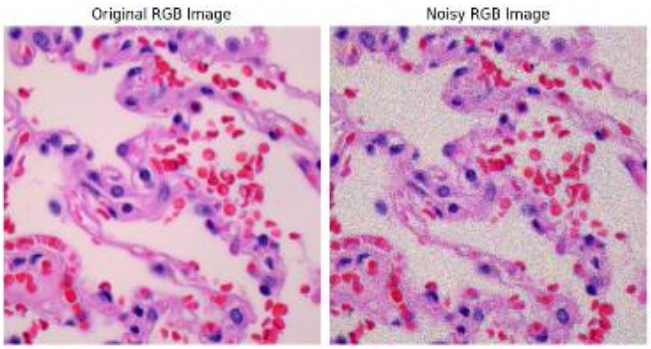

Fig. 1. Benign lung tissues biopsy: Original RGB image and noisy RGB image at noise level 4.

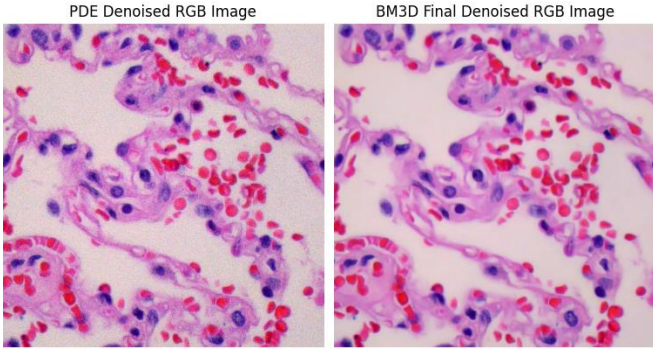

Fig. 2. Benign lung tissues biopsy: Denoised image using ACO-RFPDE (left) and Enhanced image using BM3D (right) for level 4.

Fig. 1 and Fig. 2 present a comparison between the original RGB image, the noisy RGB image at the **fourth** noise level, the image denoised using the PDE framework coupled with ACO, and the final image enhanced with BM3D.

- → Original RGB Image: This represents the clear biopsy image obtained from the LC25000 dataset, serving as the reference for comparison.
- → Noisy RGB Image: The biopsy image subjected to noise at level 4, simulating Poisson noise typically observed in real-life images.
- → PDE Denoised RGB Image: The image is processed using the proposed RFPDE-ACO framework, which removes the majority of the noise while retaining critical features.
- → BM3D Final Denoised RGB Image: The image is enhanced further using BM3D, improving feature preservation and overall clarity.

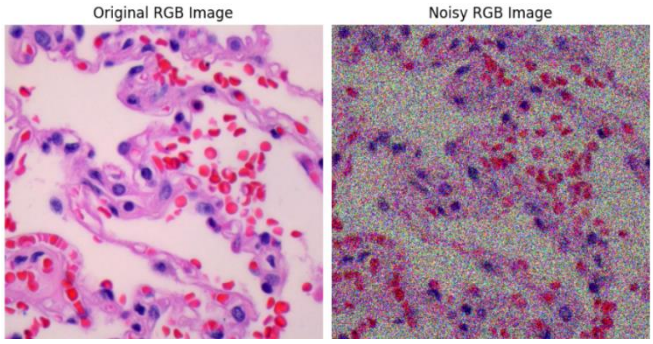

Fig. 3. Benign lung tissues biopsy: Original RGB image and noisy RGB image at noise level 6.

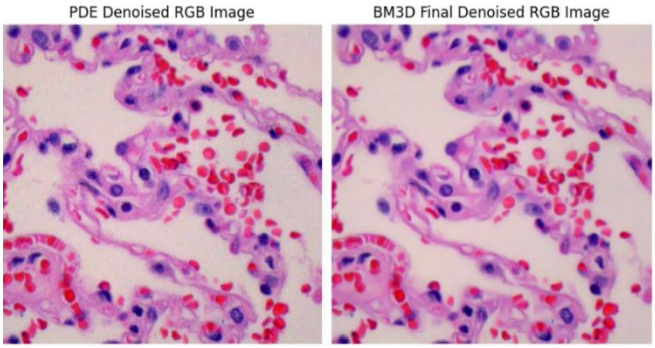

Fig. 4. Benign lung tissues biopsy: Denoised image using ACO-RFPDE (left) and Enhanced image using BM3D (right) for level 6.

Fig. 3 and Fig. 4 present a comparison between the original RGB image, the noisy RGB image at the **sixth** noise level, the image denoised using the PDE framework coupled with ACO, and the final image enhanced with BM3D.

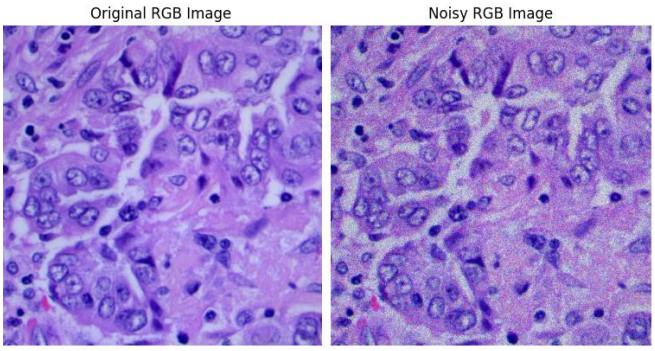

Fig. 5. Lung adenocarcinomas biopsy: Original RGB image and noisy RGB image at noise level 4.

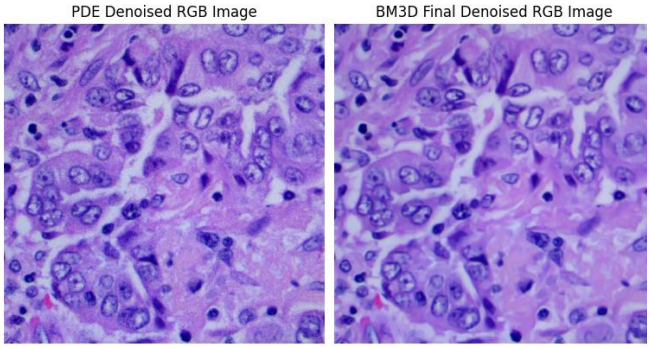

Fig. 6. Lung adenocarcinomas biopsy: Denoised image using ACO-RFPDE (left) and Enhanced image using BM3D (right) for level 4.

Fig. 5 and Fig. 6 present a comparison between the original RGB image, the noisy RGB image at the **fourth** noise level, the image denoised using the PDE framework coupled with ACO, and the final image enhanced with BM3D.

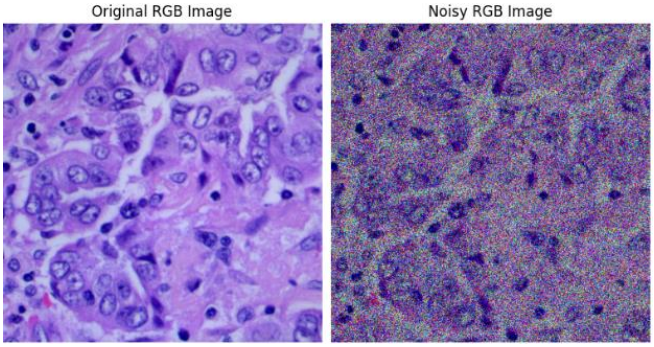

Fig. 7. Lung adenocarcinomas biopsy: Original RGB image and noisy RGB image at noise level 6.

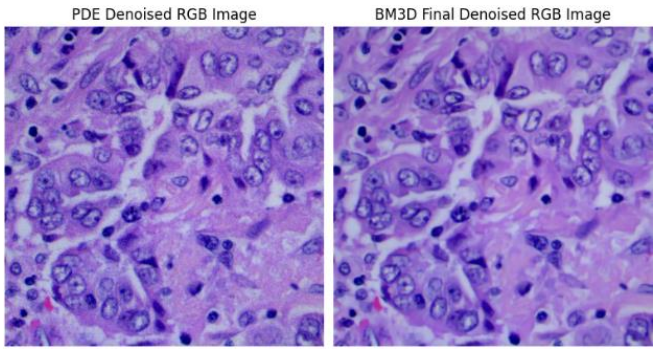

Fig 8. Lung adenocarcinomas biopsy: Denoised image using ACO-RFPDE (left) and Enhanced image using BM3D (right) for level 6.

Fig. 7 and Fig. 8 present a comparison between the original RGB image, the noisy RGB image at the **sixth** noise level, the image denoised using the PDE framework coupled with ACO, and the final image enhanced with BM3D.

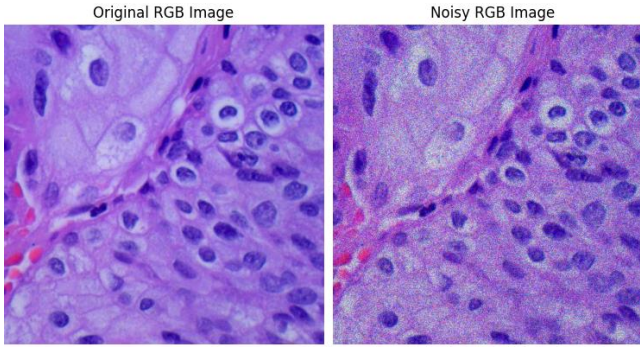

Fig. 9. Lung squamous cell carcinomas biopsy: Original RGB image and noisy RGB image at noise level 4.

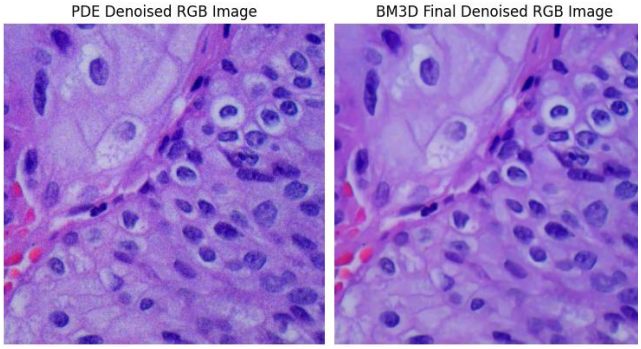

Fig 10. Lung squamous cell carcinomas biopsy: Denoised image using ACO-RFPDE (left) and Enhanced image using BM3D (right) for level 4.

Fig. 9 and Fig. 10 present a comparison between the original RGB image, the noisy RGB image at the **fourth** noise level, the image denoised using the PDE framework coupled with ACO, and the final image enhanced with BM3D.

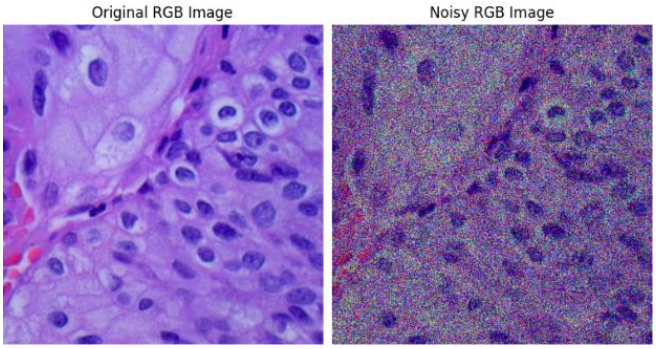

Fig. 11. Lung squamous cell carcinomas biopsy: Original RGB image and noisy RGB image at noise level 6.

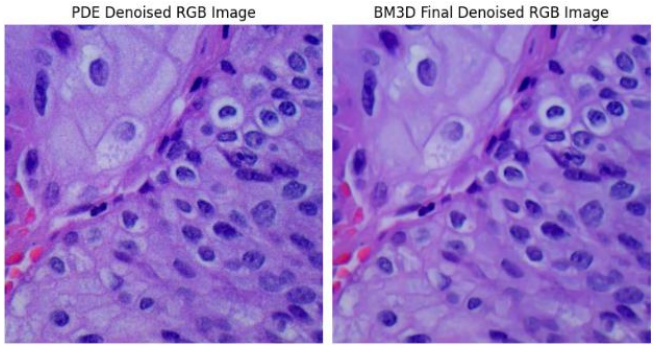

Fig 12. Lung squamous cell carcinomas biopsy: Denoised image using ACO-RFPDE (left) and Enhanced image using BM3D (right) for level 6.

Fig. 7 and Fig. 8 present a comparison between the original RGB image, the noisy RGB image at the **sixth** noise level, the image denoised using the PDE framework coupled with ACO, and the final image enhanced with BM3D.

The parameters derived from all the above images were compiled into tables to enable quantitative comparisons. This organization provides a clear understanding of how the parameters change across different stages and illustrates the impact of each stage on the overall results.

TABLE I. DESCRIPTION OF THE IMAGE QUALITY PERFORMANCE MERTICES

Metrics	Formula
MSE	$MSE = \frac{1}{PQ}\sum_{i=0}^{P-1}\sum_{j=0}^{Q-1}[u_{\text{ACORFPDE}} - u_{\text{ref}}]^2$
PSNR	$PSNR = 10\log_{10}\left(\frac{(L-1)^2}{\text{MSE}(u_{\text{ACO-RFPDE}}, u_{\text{ref}})}\right)$ db
CC	$CC = \frac{\sum(u_{\text{ref}} - \mu_{u_{\text{ref}}})\sum(u_{\text{ACORFPDE}} - \mu_{u_{\text{ACORFPDE}}})}{\sqrt{\sum(u_{\text{ref}} - \mu_{u_{\text{ref}}})^2\sum(u_{\text{ACORFPDE}} - \mu_{u_{\text{ACORFPDE}}})^2}}$
NAE	$NAE = \frac{\sum_{i=0}^{P-1}\sum_{j=0}^{Q-1}\lvert u_{\text{ref}} - u_{\text{ACO-RFPDE}}\rvert}{\sum_{i=0}^{P-1}\sum_{j=0}^{Q-1} u_{\text{ref}}}$
UQI	$UQI = \frac{4\mu_{\text{ref}}\mu_{\text{ACO-RFPDE}}\sigma_{\text{ref,ACO-RFPDE}}}{(\mu_{\text{ref}}^2 + \mu_{\text{ACO-RFPDE}}^2)(\sigma_{\text{ref}}^2 + \sigma_{\text{ACO-RFPDE}}^2)}$
SSIM	$SSIM = \frac{(2\mu_{u_{\text{ref}}}\mu_{u_{\text{ACORFPDE}}} + c_1)(2\sigma_{u_{\text{ref}}u_{\text{ACORFPDE}}} + c_2)}{(\mu_{u_{\text{ref}}}^2 + \mu_{u_{\text{ACORFPDE}}}^2 + c_1)(\sigma_{u_{\text{ref}}}^2 + \sigma_{u_{\text{ACORFPDE}}}^2 + c_2)}$

PSNR (Peak Signal-to-Noise Ratio): Measures the level of noise reduction, where higher values indicate better denoising.

SSIM (Structural Similarity Index): Assesses the structural similarity between the original and denoised images.

MSE (Mean Squared Error): Quantifies the average error or loss in image data, where lower values indicate better accuracy.

CC (Correlation Coefficient): Evaluates the degree of correlation between the original and processed images, where values closer to 1 indicate better similarity.

NAE (Normalized Absolute Error): Reflects the relative error between the original and denoised images, where lower values signify improved performance.

UQI (Universal Quality Index): Provides a comprehensive indicator of image quality, incorporating luminance, contrast, and structural fidelity.

TABLE II. COMPARATIVE QUANTITATIVE STUDY OF PARAMETERS (PSNR, SSIM, MSE, CC, NAE, AND UQI) ACROSS FIG. 1, FIG. 2, FIG. 3, AND FIG. 4

Noise level	Stage	PSNR	SSIM	MSE	NAE	CC	UQI
4	Noised	13.348	0.084	0.046	0.239	0.506	0.440
	PDE denoised	21.534	0.306	0.007	0.090	0.847	0.837
	Bm3d denoised	31.527	0.901	0.001	0.030	0.988	0.987
6	Noised	5.296	0.014	0.296	0.630	0.166	0.092
	PDE denoised	21.508	0.334	0.007	0.097	0.869	0.859
	Bm3d denoised	27.922	0.905	0.002	0.049	0.989	0.988

TABLE III. COMPARATIVE QUANTITATIVE STUDY OF PARAMETERS (PSNR, SSIM, MSE, CC, NAE, AND UQI) ACROSS FIG. 5, FIG. 6, FIG. 7, AND FIG. 8

Noise level	Stage	PSNR	SSIM	MSE	NAE	CC	UQI
4	Noised	13.387	0.0943	0.0459	0.287	0.439	0.355
	PDE denoised	21.862	0.365	0.0065	0.107	0.799	0.779
	Bm3d denoised	31.764	0.859	0.0007	0.0338	0.975	0.972
6	Noised	5.663	0.0155	0.274	0.782	0.145	0.070
	PDE denoised	22.146	0.403	0.0061	0.1191	0.832	0.816
	Bm3d denoised	29.077	0.865	0.0013	0.0490	0.977	0.9757

TABLE IV. COMPARATIVE QUANTITATIVE STUDY OF PARAMETERS (PSNR, SSIM, MSE, CC, NAE, AND UQI) ACROSS FIG. 9, FIG. 10, FIG. 11, AND FIG. 12

Noise level	Stage	PSNR	SSIM	MSE	NAE	CC	UQI
4	Noised	13.444	0.062	0.045	0.299	0.397	0.302
	PDE denoised	21.710	0.271	0.006	0.115	0.755	0.726
	Bm3d denoised	32.926	0.874	0.0005	0.031	0.977	0.974
6	Noised	5.742	0.0096	0.269	0.820	0.129	0.055
	PDE denoised	21.185	0.270	0.0077	0.1455	0.765	0.735
	Bm3d denoised	28.773	0.871	0.0014	0.0553	0.978	0.975

The values obtained from the above tables were plotted as line graphs to facilitate further quantitative evaluation of the model's performance. These plots provide a clear visual comparison of each parameter across different steps in the workflow, highlighting the progressive improvement in image quality throughout the denoising process.

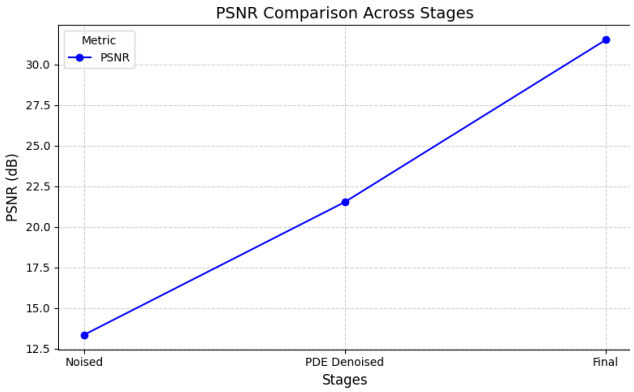

(A)

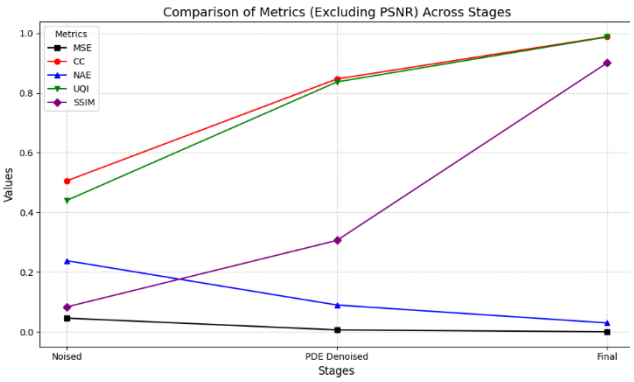

(B)

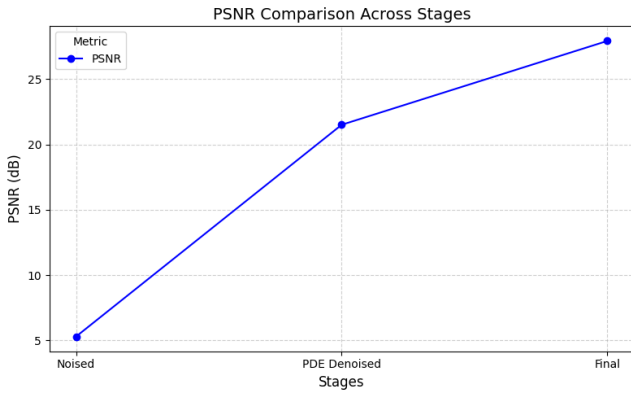

(C)

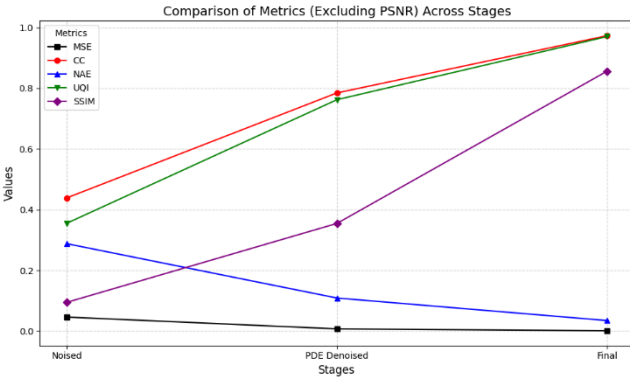

(B)

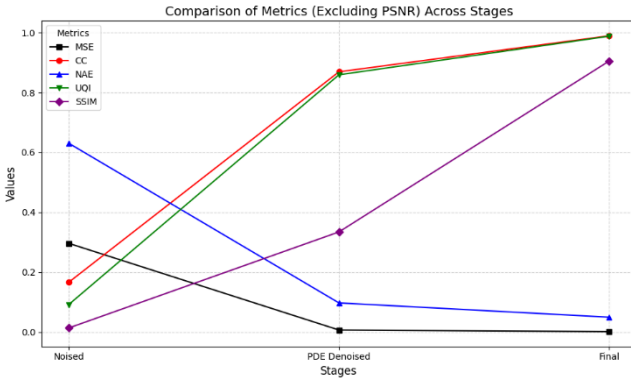

(D)

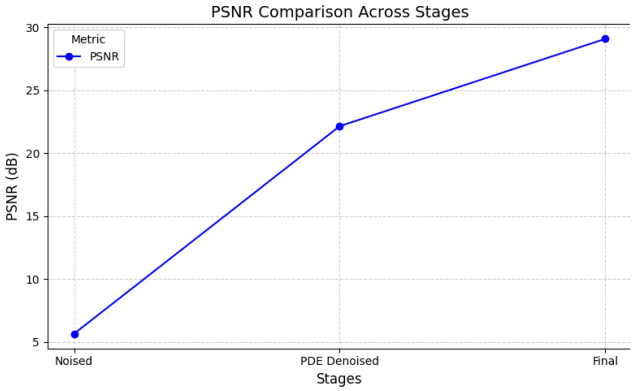

(C)

Fig. 13. Line plot representation of Table II, illustrating quantitative metrics for denoising performance: (a) PSNR at noise level 4; (b) SSIM, MSE, NAE, CC, and UQI at noise level 4; (c) PSNR at noise level 6; (d) SSIM, MSE, NAE, CC, and UQI at noise level 6.

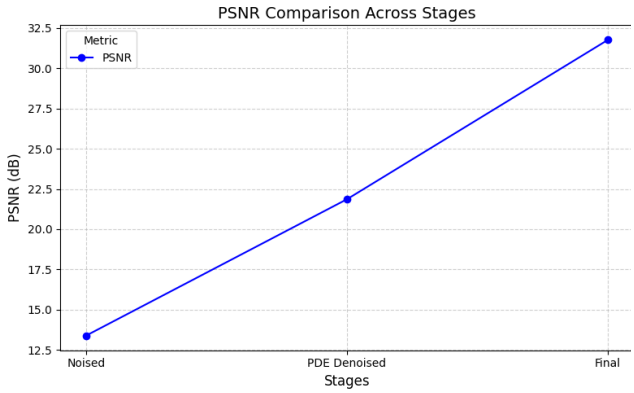

(A)

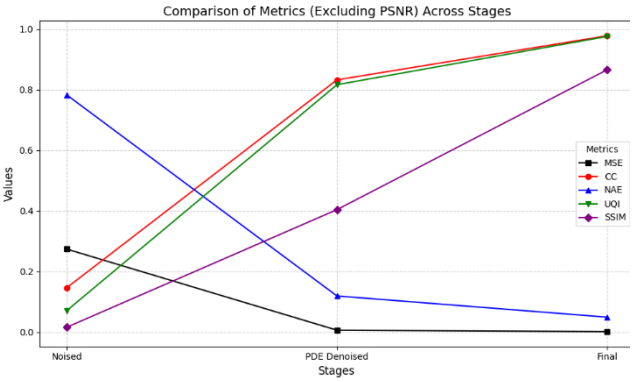

(D)

Fig. 14. Line plot representation of Table III, illustrating quantitative metrics for denoising performance: (a) PSNR at noise level 4; (b) SSIM, MSE, NAE, CC, and UQI at noise level 4; (c) PSNR at noise level 6; (d) SSIM, MSE, NAE, CC, and UQI at noise level 6.

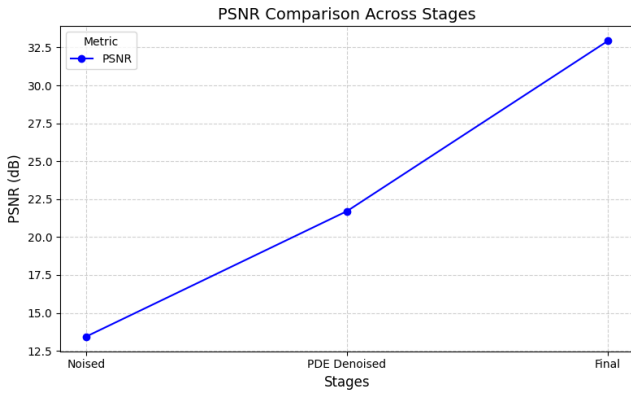

(A)

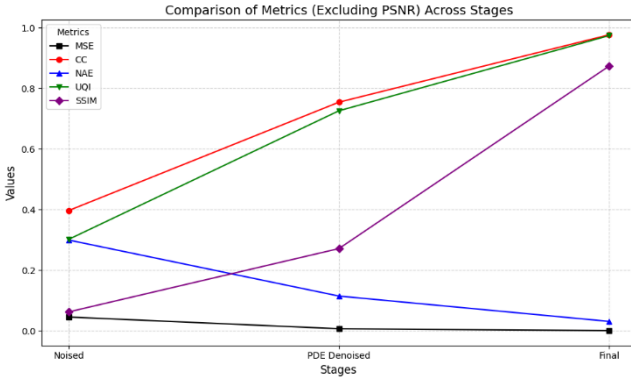

(B)

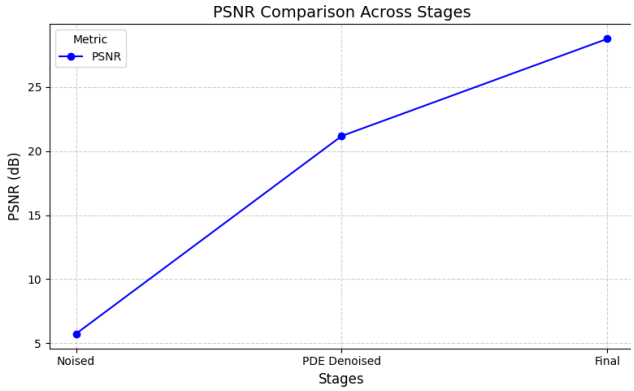

(C)

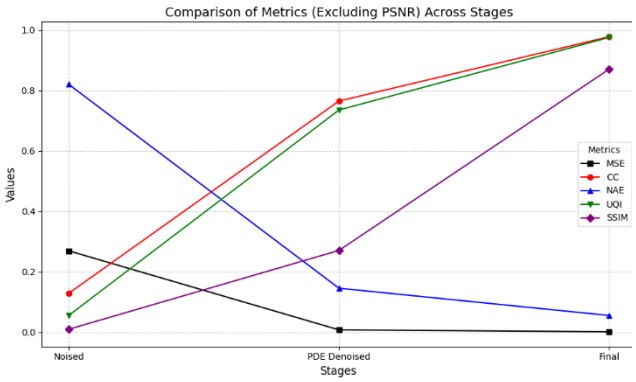

(D)

Fig. 15. Line plot representation of Table IV, illustrating quantitative metrics for denoising performance: (a) PSNR at noise level 4; (b) SSIM, MSE, NAE, CC, and UQI at noise level 4; (c) PSNR at noise level 6; (d) SSIM, MSE, NAE, CC, and UQI at noise level 6.

Finally, from the data presented, an accuracy above 95% was deduced for the framework, calculated based on the Mean Squared Error (MSE).

DISCUSSION

The results section highlights the effectiveness and efficiency of the ACO-RFPDE framework, coupled with BM3D, in enhancing the quality of biopsy images across a range of noise levels, from low to extremely high. By combining quantitative metrics (PSNR, SSIM, MSE, CC, NAE, and UQI) with qualitative visual assessments, the study offers a comprehensive evaluation of the framework's performance.

Denoising Performance at Different Noise Levels

Experiments were conducted at varying noise levels. For images with moderate noise (noise level 4), the denoising process significantly improved image clarity and preserved features. A marked increase in PSNR values was observed after applying the proposed framework and further enhancement with BM3D, indicating effective noise reduction. SSIM values demonstrated improved structural similarity, highlighting the framework's ability to retain fine details of the image. Additionally, reductions in MSE and NAE confirmed the success of the model, while higher CC and UQI values underscored the strong correlation and overall quality of the processed images.

At higher noise levels (noise level 6), Poisson noise became more prominent, obscuring finer details of the images. Despite this challenge, the framework's performance remained robust. While the initial noisy images exhibited reduced brightness and obscured features, the ACO-RFPDE framework effectively restored much of the lost detail. Quantitative metrics such as PSNR and SSIM, though slightly lower compared to noise level 4, continued to demonstrate substantial noise reduction and feature preservation. The BM3D-enhanced images maintained high CC and UQI values, reaffirming the reliability of the framework even under challenging noise conditions.

Comparative Analysis Across Different Tissue Types

The framework was tested on biopsy images from various tissue types, including benign lung tissues, lung adenocarcinomas, and lung squamous cell carcinomas. In all cases, the framework achieved significant noise reduction while preserving essential diagnostic features, as demonstrated in the quantitative tables and line plots. This consistency across different tissue types validates the adaptability and effectiveness of the proposed framework for diverse diagnostic scenarios.

CONCLUSION

The ACO-RFPDE framework coupled with BM3D demonstrated effective denoising and enhancement of medical biopsy images across varying noise levels. Applied to multiple images from the LC25000 dataset, the framework achieved significant noise reduction while preserving critical diagnostic features, with improvements observed in PSNR, SSIM, and other metrics. Even at higher noise levels, it successfully restored image quality, showcasing its reliability for clinical diagnostics. The current framework showcases effective noise reduction and image enhancement for medical biopsy images. Future work will focus on transforming the ACO-RFPDE framework into a fully automated AI-based model. This will involve training deep learning architectures on diverse biopsy datasets to generalize the denoising and enhancement process. The aim is to create a model that can adaptively learn to handle varying noise levels and tissue types while maintaining computational efficiency and diagnostic accuracy. Additionally, efforts will be directed toward integrating this AI model into clinical workflows to assist pathologists in real-time diagnostic applications.

References

[1] S.S. Hecht, Tobacco smoke carcinogens and lung cancer, Curr. Cancer Res. 6 (2011) 53–74, https://doi.org/10.1007/978-1-61737-995-6_3.

[2] B. Prabhakar, P. Shende, S. Augustine, Current trends and emerging diagnostic techniques for lung cancer, Biomed. Pharmacother. 106 (2018) 1586–1599, https://doi.org/10.1016/j.biopha.2018.07.145.

[3] V. G¨oreke, A novel method based on Wiener filter for denoising Poisson noise from medical X-Ray images, Biomed. Signal Process. Control. 79 (2022), https://doi.org/10.1016/j.bspc.2022.104031.

[4] S.C. Huang, Y.T. Peng, C.H. Chang, K.H. Cheng, S.W. Huang, B.H. Chen, Restoration of images with high-density impulsive noise based on sparse approximation and ant-colony optimization, IEEE Access 8(2020) 99180–99189, https://doi.org/10.1109/ACCESS.2020.2995647

[5] R. Kumar, S. Srivastava, R. Srivastava, A fourth order PDE based fuzzy c- means approach for segmentation of microscopic biopsy images in presence of Poisson noise for cancer detection, Comput. Methods Programs Biomed. 146 (2017) 59–68, https://doi.org/10.1016/j.cmpb.2017.05.003.

[6] S. Srivastava, R. Srivastava, N. Sharma, S.K. Singh, S. Sharma, A fourth-order PDE-based non-linear filter for speckle reduction from Optical Coherence Tomography images, Int. J. Biomed. Eng. Technol. 10 (2012) 55–69.

[7] T. Le, R. Chartrand, T.J. Asaki, A variational approach to reconstructing images corrupted by poisson noise, J. Math. Imag. Vis. 27 (2007) 257–263, https://link.springer.com/article/10.1007/s10851-007-0652-y.

[8] R. Srivastava, S. Srivastava, Restoration of Poisson noise corrupted digital images with nonlinear PDE based filters along with the choice of regularization parameter estimation, Pattern Recognit. Lett. 34 (2013) 1175–1185, https://doi.org/ 10.1016/j.patrec.2013.03.026.

[9] Prem Chand Yadava, Subodh Srivastava, Denoising of poisson-corrupted microscopic biopsy images using fourth-order partial differential equation with ant colony optimization, Biomedical Signal Processing and Control, https://doi.org/10.1016/j.bspc.2024.106207.

[10] A. Kumar, P. Kumar, S. Srivastava, A skewness reformed complex diffusion based unsharp masking for the restoration and enhancement of Poisson noise corrupted mammograms, Biomed. Signal Process. Control. 73 (2022) 103421, https://doi.org/10.1016/j.bspc.2021.103421.

[11] Y.F. Pu, Fractional-order euler-lagrange equation for fractional-order variational method: a necessary condition for fractional-order fixed boundary optimization problems in signal processing and image processing, IEEE Access. 4 (2016) 10110–10135, https://doi.org/10.1109/ACCESS.2016.2636159.

[12] J. Tian, W. Yu, S. Xie, An ant colony optimization algorithm for image edge detection, in: 2008 IEEE Congr. Evol. Comput. CEC 2008, 2008, pp. 751–756, https://doi.org/10.1109/CEC.2008.4630880.

[13] https://pypi.org/project/bm3d/

[14] A.A. Borkowski, M.M. Bui, L.B. Thomas, C.P. Wilson, L.A. DeLand, S.M. Mastorides, Lung and Colon Cancer Histopathological Image Dataset (LC25000), (2019) 1–2. http://arxiv.org/abs/1912.12142.

--